# The darkening of copper- or lead-based pigments explained by a structural modification of natural orpiment : a spectroscopic and electrochemical study

The darkening of copper- or lead-based pigments by arsenic sulfide pigments explained through a structural modification of natural orpiment: a spectroscopic and electrochemical study.

Marc Vermeulen[1, 2], Jana Sanyova[1], Koen Janssens[2], Gert Nuyts[2], Steven De Meyer[2] and Karolien De Wael[2].

[1] Polychrome Artefact Laboratory, Royal Institute for Cultural Heritage, Parc du Cinquantenaire 1, B-1000 Brussels, Belgium

[2] AXES research group, University of Antwerp, Campus Groenenborger, B-2020 Antwerp, Belgium

**Abstract**

A combined Raman and electrochemical study of natural orpiment ($As_2S_3$), an arsenic sulfide pigment, was used to assess the quick formation of oxidized species such as arsenic oxide ($As_2O_3$) upon exposing the pigment to 405 nm or 532 nm monochromatic lights while simultaneously recording the Raman spectra of the exposed sample. During this process, a distortion of the main band at 355 $cm^{-1}$, associated with the stretching of $AsS_{3/2}$ pyramids of natural orpiment was observed as well as an increased intensity of the 359 $cm^{-1}$ band, corresponding to covalent As-As bonds in natural orpiment. The distortion was accompanied by an overall decrease of the global Raman signal for natural orpiment, which could be explained by a loss in crystal structure. The same phenomena were recorded in reference natural orpiment model paint samples stored for a long time together with verdigris and minium ($Pb_3O_4$) paints, the two latter appearing darkened on their sides closest to the orpiment sample as well as in several historical samples containing natural orpiment mixed with various blue pigments. By SEM-EDX and XRPD analysis, respectively on loose material and cast thin-section of model paint samples, the darkening was identified as dark sulfide species such as chalcocite ($Cu_2S$) and galena (PbS), suggesting the release of volatile sulfide or related species by the natural orpiment paint. XANES analyses of paint samples presenting As-As bond increase indicated the presence of sulfur species most likely identified as organosulfur compounds formed upon the As-As bond formation and explained the darkening of the Cu- and Pb-based pigments. To the authors best knowledge, this article reports for the first time the light-induced formation of As-As bonds in natural orpiment used as an artists' pigment and objectively demonstrates the incompatibility between orpiment and (arsenic) sulfide-sensitive pigments.

**Introduction**

Photochemically- and atmospherically-induced alterations in artists' pigments are the result of well-known degradation processes. These alterations can often be visually perceived as color changes, either caused by a change in the oxidation state in the original material or the formation of degradation products or salts, via complex reactions.[1–4] Also arsenic-based pigments such as natural orpiment ($As_2S_3$) or natural realgar ($\alpha$-$As_4S_4$) are not immune to such modifications and are often described as easily oxidizing upon light exposure.[5–8] Upon aging, they have often been described to darken adjacent copper- and lead-based pigments due to the alleged formation of copper(I) sulfide (chalcocite, $Cu_2S$) or lead(II) sulfide (galena, PbS) due to a reaction with unidentified sulfide compounds emitted upon decomposition of arsenic sulfides.[6,9–11] While the exact mechanism behind the sulfide formation, which is essential for the reaction, still remains unclear, it is well documented that natural orpiment ($As_2S_3$, golden yellow) directly transforms into arsenic oxide

($As_2O_3$, white) while natural realgar (α-$As_4S_4$, orange-red) first turns into pararealgar (ß-$As_4S_4$, yellow) before oxidizing into arsenic oxide.[6,12–17] It is important to note that this oxidation process does not modify the oxidation state of the arsenic (+3) in the unaltered pigment and in the arsenic oxide. Nonetheless, recent studies showed that in a humid environment hydrated arsenic trioxide ($H_3AsO_3$) may degrade into arsenate compounds (+5); the latter have been recently identified in paint cross-sections by means of X-ray absorption near edge structure (XANES) spectroscopy. [18,19]

The transformation of realgar to pararealgar is well described in literature as a structural modification in which, under the influence of light and oxygen, a sulfur atom is inserted between two arsenic atoms of the realgar cage leading to a metaphase called uzonite (χ-phase, $As_4S_5$) and arsenic oxide ($As_2O_3$). This metaphase will later decompose into ß-$As_4S_4$ by breaking an As-S-As bond and releasing a sulfur atom (radical) (Eq. 1 and 2) [15,16,20–23].

$5\ \alpha\text{-}As_4S_4\ (\text{realgar}) + 3\ O_2 \rightarrow 4\ As_4S_5\ (\text{uzonite, }\chi\text{-phase}) + 2\ As_2O_3$ (Eq. 1)

$As_4S_5\ (\text{uzonite, }\chi\text{-phase}) \rightarrow \beta\text{-}As_4S_4\ (\text{pararealgar}) + S$ (Eq. 2)

Through the release of the sulfur atom (radical), the process can continue via a set of cyclic reactions in which the sulfur reacts again with a molecule of realgar to produce a molecule of pararealgar whereupon a new sulfur radical is produced to continue the process:

$S + \alpha\text{-}As_4S_4\ (\text{realgar}) \rightarrow As_4S_5\ (\text{uzonite, }\chi\text{-phase})$ (Eq. 3)

$As_4S_5\ (\text{uzonite, }\chi\text{-phase}) \rightarrow \beta\text{-}As_4S_4\ (\text{pararealgar}) + S$ (Eq. 4)

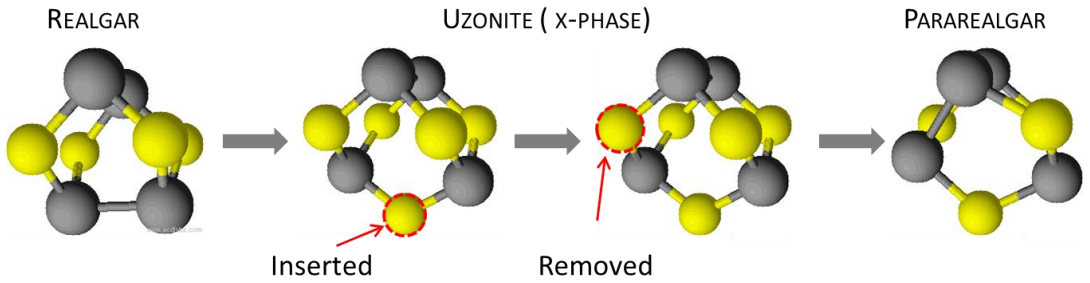


**Figure 1. Schematic representation of the transformation of realgar into pararealgar via the uzonite χ-phase $As_4S_5$ according to Kyono *et al.*, 2005. The arrows show the processes of the phase transformation. As and S atoms are respectively represented in black and yellow spheres.**

Even though this photo-induced modification of the crystalline structure has been described quite extensively for realgar, a similar process has never been observed with natural orpiment. The degradation process for the latter has often been described as a direct oxidation of the sulfide pigment into arsenic oxide ($As_2O_3$) (Eq. 5). [6,13]

$As_2S_3 + 3\ O_2 \rightarrow 2\ As_2O_3 + 6\ S$ (Eq. 5)

In view of their excellent Raman scattering properties, arsenic sulfide pigments and their degradation products are frequently studied with Raman spectroscopy.[21,22,24,25] Nonetheless, electrochemistry has recently been used to examine the degradation products and mechanisms of semiconducting pigments by recording their photocurrent after exposure to monochromatic light.[26–28] This allows to quickly visualizing the changes in the pigments' photo-activity which are closely related to their

stability and degradation. As a semiconducting material, natural orpiment stability and degradation can be studied with this technique. Therefore, in this study the two aforementioned techniques were coupled in order to simultaneously monitor the variation in photo-induced current and the structural changes and degradation products of natural orpiment following exposure to light of different wavelengths.

## Materials and methods

*Historical and mock-up paint samples*

For this study, three historical samples (small paint chips cast as cross-sections) were investigated. One was taken on a Middle Empire (ca. 2000 BC) Egyptian canopic jar (Figure 2a) for which natural orpiment bound in gum arabic was used on the whole face of the lid; due to its grey appearance and its friability, this material appeared degraded. The second one was sampled on *Descent from the Cross*, an oil painting on canvas in the style of Peter Paul Rubens (with contested attribution; 1577-1640, Figure 2b); the natural orpiment was mixed with indigo and did not show any sign of degradation. The third sample originated from a French 18$^{th}$ century *Chinoiserie* oil painting (unknown artist; Figure 2c); here the orpiment was mixed with Prussian blue in order to obtain the green color of the landscape and did not present any sign of degradation. The samples were prepared as embedded cross-sections (respectively H1, H2 and H3) in order to be analyzed. The loose sample was first fixed on a 1 cm$^3$ poly(methyl methacrylate) (PMMA) cube using a white poly(vinyl acetate) (PVA) glue, after which the acrylic copolymer resin (Spofacryl®, SpofaDental, Prague) was poured on the sample and a second PMMA cube placed on top and left to dry. . Cross-sections were polished until the sample surface was exposed, first with wet polish and finished dry with Micromesh® polishing cloths up to 12 000 mesh (Scientific Instruments Services Inc., MN).


**Figure 2. Photographs of (a) the lid of the Egyptian Canopic jar (ca. 2000 BC) presenting the degraded natural orpiment layer on the face, (b) *Descent from the Cross* in the style of Peter Paul Rubens (attrib.(?), 1577-1640), in which the orpiment was mixed with indigo to obtain the green hue of the layer and (c) the 18$^{th}$-century French *Chinoiserie* painting (ca. 1700s) with the orpiment mixed with Prussian blue in the green area of the landscape. The H1, H2 and H3 sampling locations are also reported.**

In order to better understand the role of arsenic-containing pigments on the darkening of close-by lead- or copper-containing pigments, a series of mock-up paint samples were prepared in 2013 by

Brian Baade (University of Delaware) by individually mixing natural orpiment ($As_2S_3$), verdigris ($Cu(OH)_2 \cdot (CH_3COO)_2 \cdot 5\ H_2O$) and minium ($Pb_3O_4$) (Kremer Pigmente GmbH & Co, Aichstetten, Germany) in various proteinaceous binders, casein, egg yolk, egg white and sturgeon glue, the latter being used in the frame of this research. The paints were applied on a base of calcium carbonate on chalk/glue primed glass slides, stored in closed microscope slide storage boxes and kept at room temperature in the laboratory of the scientific department of the Metropolitan Museum of Art, New York for natural aging. Minium and verdigris samples were placed contactless next to the natural orpiment. Samples were taken after a 1 year period of natural dark/light aging. A summary of all the used samples can be found in table 1.

**Table 1. Description of the historical and mock-up paint samples used for the study**

| Sample | Sample description | Painting or mock-up information |
|---|---|---|
| H1 | Visually degraded yellow face | Egyptian Canopic jar by unknown artist, ca. 2000 BC |
| H2 | Bluish green area of the dress | "Descent from the Cross" in the style of Peter Paul Rubens (with contested attribution), 1577-1640 |
| H3 | Protrusion from the green area of the vegetation | "Couple in a garden" by an unknown artist, 18th c. |
| M1 | Visually unaltered natural orpiment | Aged (1 year) mock-up paint sample (pigment in sturgeon glue) prepared in 2013 by Brian Baade (University of Delaware) and conserved in the laboratory of the scientific department of the Metropolitan Museum of Art, NYC, USA |
| M2 | Darken verdigris from the edge close to the orpiment sample | |
| M3 | Darken minium from the edge close to the orpiment sample | |

*Scanning electron microscopy with energy dispersive X-ray analysis*

Backscattered electron images and elemental distribution maps were collected via Scanning electron microscopy with energy dispersive X-ray analysis (SEM-EDX), using a Zeiss - EVO LS15 SEM equipped with a Bruker EDS detection system, all operated under variable pressure vacuum. Images and elemental maps were recorded using an acceleration voltage of 15 kV, and 8 to 10 mm working distance. Data was collected and processed using the AZtecEnergy software system, v. 2.1 (Oxford Instruments).

*Micro-Raman spectroscopy*

Micro-Raman spectroscopy (μ-RS) spectra were acquired with a Renishaw inVia Raman microscope with a Peltier-cooled (203 K), near-infrared enhanced, deep-depletion CCD detector (576 × 384 pixels) using a high power 785 nm diode laser (Toptica Photonics XTRA, Graefelfing (Munich), Germany) in combination with a 1200 l/mm grating. The instrument was calibrated using a silicon wafer. Based on the particle size, samples were analyzed using the 50x or 100x objectives in a direct-coupled Leica DMLM microscope with enclosure. To avoid degradation or heat induced physical changes, the power on the samples was reduced to 0.3 mW with neutral density filters. A sample exposure time of 10 seconds (1 accumulation) was employed, resulting in an adequate signal-to-noise ratio. Spectra were acquired using the Wire 4 Raman software and were normalized into the range [0,1] in order to better visualize the broadening of the main pigment band.

*Electrochemical setup*

Natural orpiment from Kremer Pigmente GmbH & Co (Aichstetten, Germany) was used for the electrochemical study. 5 mg of the ground pigment was suspended in 1 mL of absolute ethanol; 2 µL of the orpiment-ethanol suspension was deposited on a screen-printed carbon electrode (DropSens, Llanera (Asturias) Spain). The surface of the prepared electrode was left to dry prior to the electrochemical measurements. At the beginning of the experiment, 40 to 200 µL of a 0.01 M NaCl solution was deposited on the surface of the electrode. Measurements were acquired using a µ-Autolab potentiostat from Metrohm (The Netherlands), controlled by NOVA 1.10 software. Samples were illuminated with 30 mW blue (405 nm) or green (532 nm) lasers in order to induce a measurable photocurrent.

*Raman - electrochemical coupled set-up*

The Raman-electrochemical setup was realized by coupling the above-described electrochemical setup to a Raman spectrometer. Raman spectra were collected with an inVia spectrometer (Renishaw PTY Ltd.) using a laser operating at 785 nm (red) with maximum laser output power of 240 mW. The grating was calibrated using the 520 $cm^{-1}$ silicon band. An integration time of 10 seconds (1 accumulation) and a 0.6 mW laser power (1% of the maximum power) were used. Spectra were acquired using the Renishaw WiRE 2.0 software.

The binder-free pigment deposited onto the screen-printed carbon electrode was artificially aged by irradiating the electrode for up to 60 minutes to an external blue (405 nm) or green (532 nm) laser during which the photocurrent was measured. Simultaneously, Raman spectra of the irradiated sample were recorded by means of a 785 nm red laser (Figure 3). We assume here that the Raman laser induces negligible additional damage compared to the blue and green lasers given its spectral absorption [6].

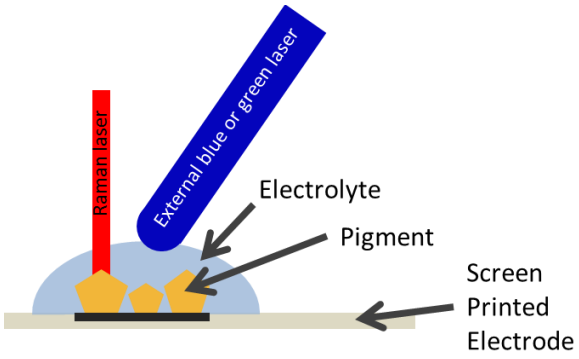


**Figure 3. Schematic representation of the Raman/electrochemistry setup.**

Similarly, binder-free natural orpiment particles were aged for 50 hours in dry conditions (no electrolyte). The aging consisted of blue (405 nm) or green (534 nm) lasers illuminations of various power (12 and 30 mW) allowing the assessment of the laser power and wavelength influence on the structure modification.

*Microscopic X-ray absorption near edge structure*

Microscopic X-ray absorption near edge structure (µ-XANES) at the S K-edge experiments were performed at the Phoenix Beamline of the Swiss Light Source (SLS, Villigen, CH). The beam size experiment was approximately 2.5 x 2.5 µm². XANES spectra were collected in the energy range 2385-2668 eV with energy increments of 1 eV. The Athena software package[29] was used to process all the XANES spectra and measure the white line intensities.

*Microscopic X-ray powder diffraction (µ-XRPD)*

µ-XRPD experiments were performed at the P06 beamline of the PETRA-III Synchrotron (DESY, Hamburg, Germany). The beam size used for this experiment was ca 0.3 x 0.5 µm². XRPD patterns were recorded using an energy of 21 keV.

**Results and discussion**

1. Characterization of the darken areas in the naturally aged mock-up paint samples

Darkened areas were observed for verdigris and minium mock-up paint samples stored together with natural orpiment and aged naturally. However, the darkening does not appear homogeneous and only is only found along the edges closest to the natural orpiment samples (Figure 4ab). Along with the darkening of the minium and verdigris samples observed, a characteristic smell of $H_2S$ ("rotten-egg" odor) was perceived upon opening of the boxes in order to realize the sampling for analysis.

SEM-EDX analysis on the loose verdigris sample (M2, Figure 4c) showed an increased presence of sulfur in the darkened areas. This is to be expected when analyzing dark copper sulfide such as chalcocite ($Cu_2S$) as verdidris, a copper acetate, does not contain any sulfur ($Cu(OH)_2 \cdot (CH_3COO)_2 \cdot 5 H_2O$). However, for the minium degradation product, SEM-EDX could not be used due to the difficulty in differentiating sulfur and lead. Therefore, other identification techniques such as x-ray diffraction were considered for characterizing the darkened fraction of the minium sample (M3). µ-XRPD analysis on a thin section of the minium paint sample was carried out at the PETRA-III Synchrotron (DESY, Hamburg, Germany) and allowed the identification of the dark degradation product as galena (PbS), present along with non-degraded minium ($Pb_3O_4$) (Figure 4d,e).

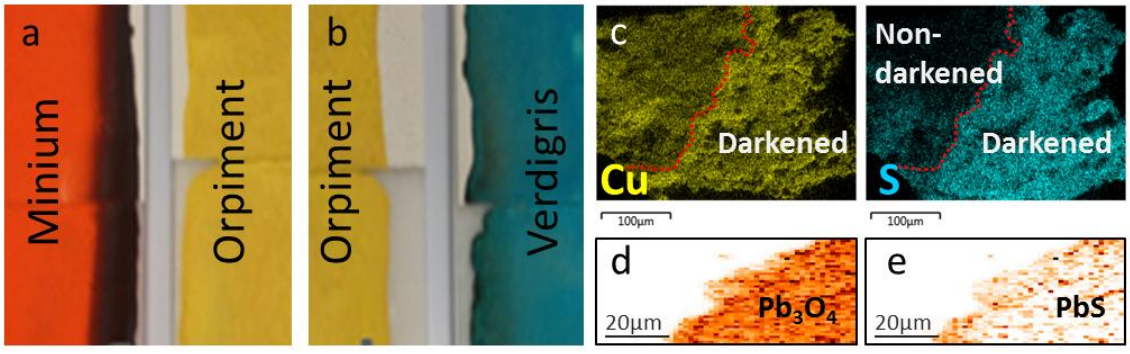


**Figure 4. Mock-up sample of a) minium and natural orpiment and b) natural orpiment and verdigris all bound in sturgeon glue and stored contactless in a closed box. The areas of minium and verdigris closest to the orpiment appear darkened and were revealed to contain a significantly larger amount of sulfur according to SEM-EDX analysis on M2 (c). By means of µ-XRPD scanning of M3, not only $Pb_3O_4$ (d) but also PbS (galena) was revealed (e).**

2. Formation of covalent As-As bonds in natural orpiment

While the SEM backscattered images of two historical samples (H1 and H2) present the characteristic layered structure expected for natural orpiment (Figure 5a)[5,6], the Raman spectra of all three historical samples H1-H3 revealed a striking feature when compared to reference spectrum (Figure 5b): the main band for the pigment's $AsS_{3/2}$ pyramids at 355 $cm^{-1}$ appears distorted. On intensity normalized spectra, the distortion either causes a shift of the band toward higher wavenumbers (Figure 6b-2, 6d-2 and 6f-2) or may be observed as an inversion of the main contribution and shoulder (Figure 6b-3, 6d-3 and 6f-3). When comparing the bandshape/position of the core of the pigment particles to their surface (Figures 6a, 6c and 6e), it becomes clear that the spectrum from the core of the pigment (Figures 6b-1, 6d-1 and 6f-1) is representative of unaltered natural orpiment (Figure 5b) while the outer shell has a stronger distorted signal at 359 $cm^{-1}$ compared to the 355 $cm^{-1}$ contribution. The mid-section presents contributions for both 355 and 359 $cm^{-1}$ of comparable intensity (Figures 6b-2, 6d-2 and 6f-2), explaining the broad band observed.

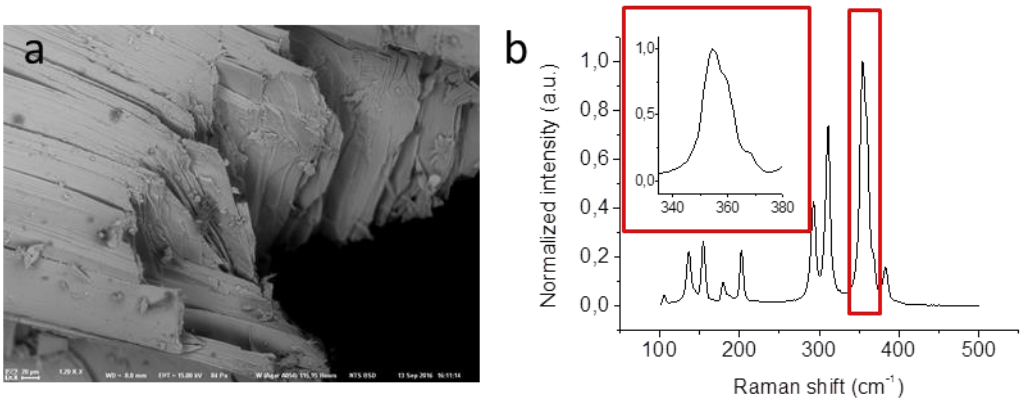


**Figure 5. Backscattered electron image showing the layered structure of natural orpiment (a) and its Raman spectrum (b). The insert corresponds to the stretching vibration of the $AsS_{3/2}$ pyramids.**

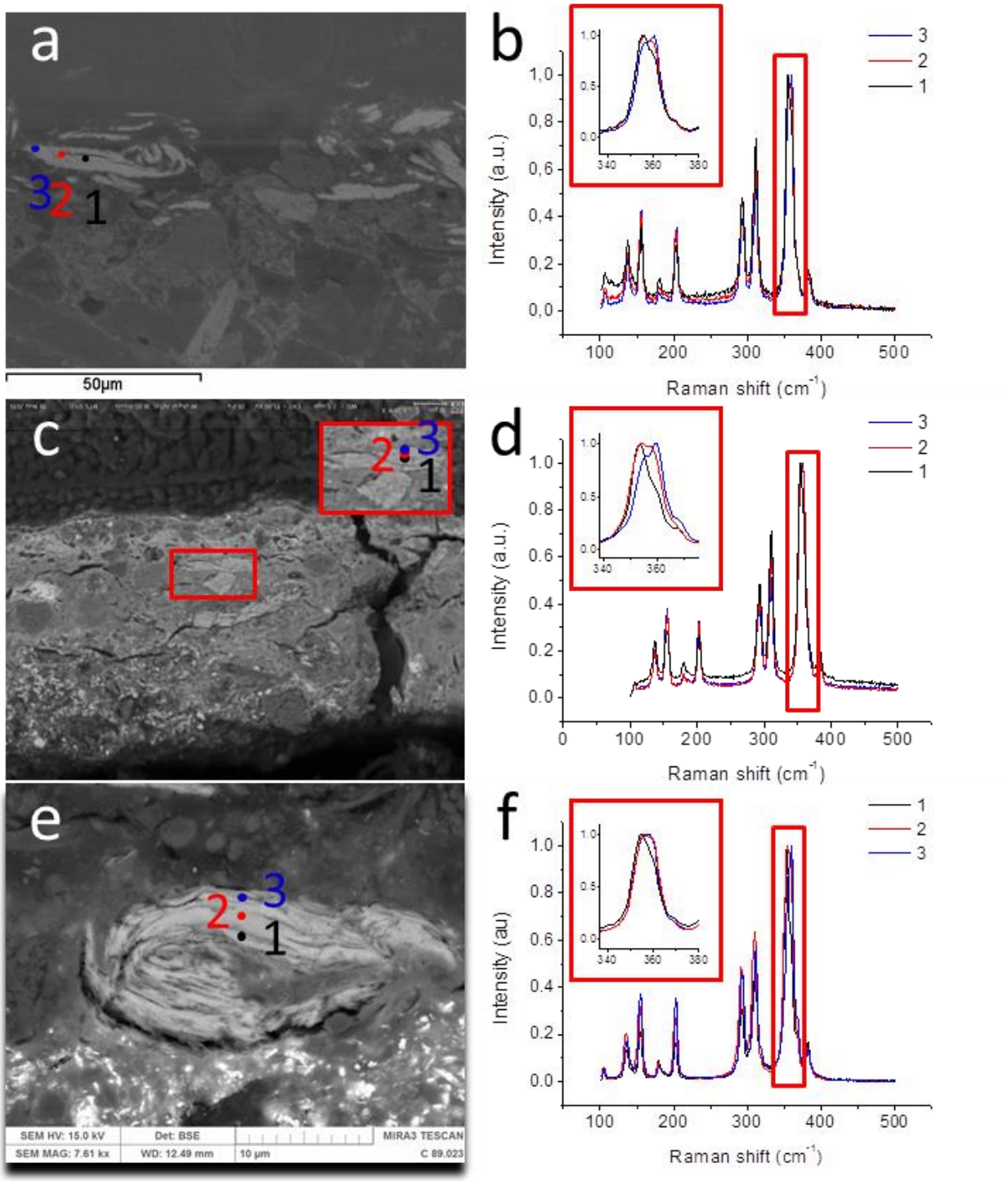


**Figure 6. Backscattered electron images of the historical samples a) sample H1 (canopic jar), c) sample H2 (green areas in "Rubens" painting) and e) sample H3 (green mixture from foliage in *Chinoiserie*) . Points 1, 2 and 3 are the locations of Raman spot analyses (b, d and f) at the core and surface of the orpiment grains, showing the split in the $AsS_{3/2}$ pyramid band (inserts).**

The same features can be observed in the Raman data obtained on the orpiment mock-up samples (M1) stored alongside the minium and verdigris. When looking at the normalized intensity spectra, the area of the orpiment-containing layer most exposed to light presents a higher contribution of the band at 359 $cm^{-1}$ compared to the unaltered pigment encountered deeper in the pigment particle (Figure 7a). Furthermore, in the non-normalized intensity spectra (Figure 7b), a depth-dependent

variation of the Raman signal for natural orpiment was recorded. Spectra 1 and 2 in Figure 7b were collected in the deep- and mid-orpiment layer and exhibit a Raman signal very close to unaltered natural orpiment. When moving toward the surface (spectra 3, 4 and 5 in Figure 7b), a broadening of the band is observed due to an increasing contribution of the 359 $cm^{-1}$ band and a continuous decrease in the overall Raman signal is noticed. This overall Raman signal decrease could be explained by the formation of arsenic oxide at the expense of natural orpiment, thus reducing the quantity of Raman scattering natural orpiment. For both the historical and mock-up samples no other band modification is observed in the Raman spectrum of natural orpiment, except for the changes observed in the 355-359 $cm^{-1}$ range. No characteristic 367 $cm^{-1}$ As-O-As bending vibration band for arsenolite ($As_2O_3$), a degradation product expected to be formed here, were observed.

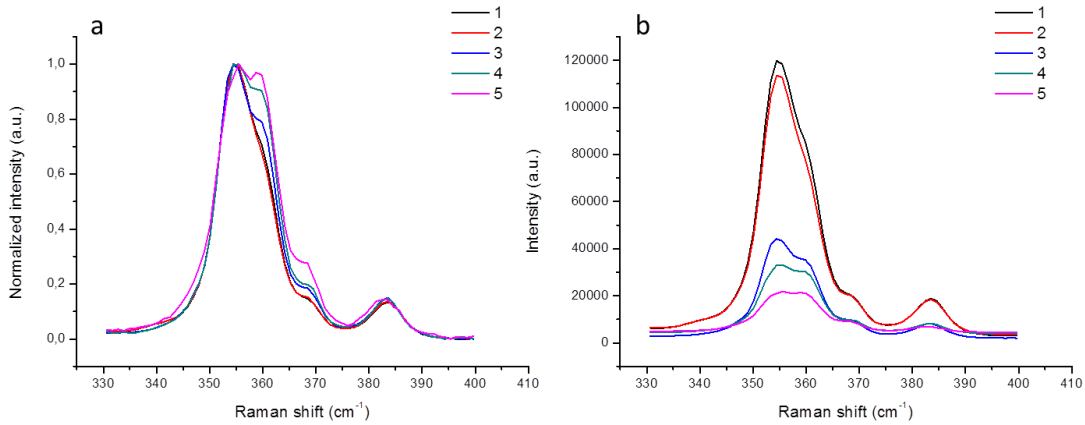


**Figure 7. a) Normalized intensity and b) non-normalized Raman spectra of natural orpiment in sturgeon glue (M1). (1) and (2) were collected in the deeper part of the orpiment layer while (3), (4) and (5) were collected moving toward the surface.**

The split in the Raman signal corresponding to the stretching vibrations of the $AsS_{3/2}$ pyramids of orpiment, observed in Figures 6 and 7, can be attributed to the formation of covalent As-As bonds. This bond formation has been described for the light-induced transformation of realgar to pararealgar[20] as well as for the light-induced alteration of artificial arsenic sulfide glass[30,31]. However, this phenomenon has never been described for natural orpiment nor has it been associated with the *in situ* formation of a degradation phase in painted works of art. Since Raman intensities are usually directly proportional to the concentration of the active species[32,33], the general decrease in Raman intensity for orpiment when this As-As linkage increases (as observed in Figures 6 and 7) suggests that this bonding phenomenon is altering the crystalline structure of the natural pigment. µ-XRDP analyses (carried out at beamline P06, PETRA-III, Hamburg, Germany) on the natural orpiment mock-up paint sample M1 revealed that next to natural orpiment ($As_2S_3$), arsenic oxide ($As_2O_3$) was present (Figure 8). A clear contrast between the non-degraded and degraded parts of the paint could be identified (Figure 8b) suggesting a loss of crystalline natural orpiment in the most exposed surface; and a greater concentration of arsenic oxide is found along the exposed surface (Figure 8c). No other crystalline phases were identified by means of µ-XRPD which may suggest the formation of a non-crystalline organic phase. Arsenic oxide may have gone undetected in Raman spectroscopy due to a concentration below the technique's detection limit for such compounds.

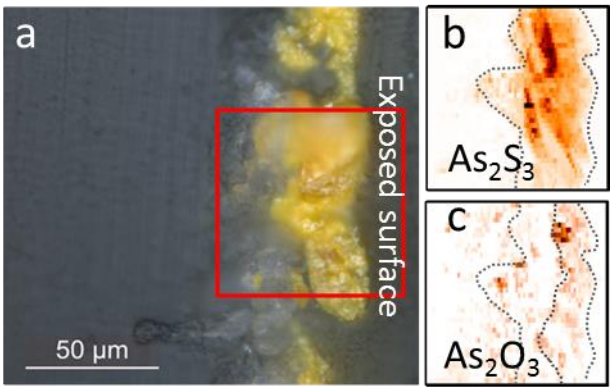


**Figure 8. Cross-section photomicrograph of the natural orpiment/sturgeon glue mock-up sample (M1) from the Metropolitan Museum of Art (a) and µ-XRPD analysis of the selected area highlighting the presence of natural orpiment (b) and arsenolite (c).**

The increase of the 359 $cm^{-1}$ band, coupled with the overall decrease of the Raman and XRPD signal when moving from the core toward the exposed surface of the pigment grain suggests, similar to what has been described for realgar and amorphous arsenic sulfides, that a light-induced phenomenon takes place. Nonetheless, reactions involving the binder or other external chemical agents may also be occurring and cannot be excluded. Therefore, the behavior of the orpiment was further investigated by means of the Raman-electrochemical setup.

Binder-free pigment deposited on screen-printed electrodes were irradiated over an increasing time period by a green laser to mimic light induced ageing., while simultaneously Raman spectra were collected. Figures 9a and 9b present a progressive split in the main orpiment band (355 $cm^{-1}$) as a function of green laser irradiation: the intensity of the As-As band at 359 $cm^{-1}$ increases. This result is consistent with the phenomenon observed in the historical (H1-H3) and natural orpiment mock-up sample (M1) analyzed for this study. Besides the 355-359 $cm^{-1}$ split, two new bands at 193 and 330 $cm^{-1}$ can be identified (Figure 9a). However, Figure 9c suggests that these two bands are most likely due to the scattering of the green laser used for the simultaneous artificial aging as they are found when the electrode is illuminated with the external green laser in presence or not of the pigment. However they are not found when the setup is not illuminated (Figure 9c – orpiment red laser) or illuminated with a blue laser (Figure 9d)

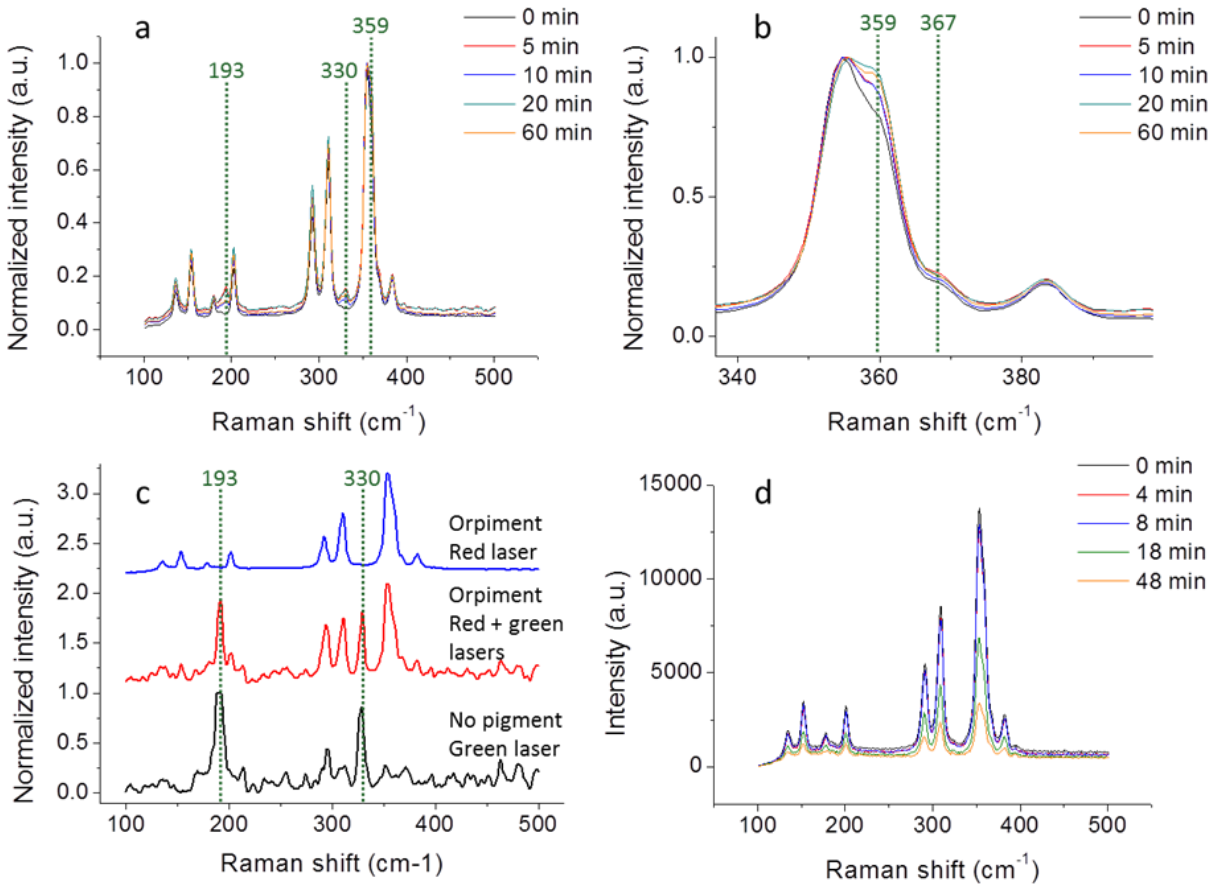


**Figure 9. Time series of Raman spectra obtained from (a,b) green laser illuminated natural orpiment presenting the increasing split in the 355-359 $cm^{-1}$ region and two laser-induced scattering bands at 193 and 330 $cm^{-1}$; (c) the two laser-induced scattering bands at 193 and 330 $cm^{-1}$ obtained by illuminating the electrode with a green laser; and d) from blue laser illumination showing an overall decrease of the Raman signal.**

The formation of As-As bonds is observed in all analyzed samples, i.e. independent of the binding medium employed (gum arabic for H1, oil for H2 and H3, and glue for the naturally aged mock-up sample M1) as well as in the binder-free orpiment exposed to green laser light (Figure 9). Furthermore, no indication of As-As bond formation is found in the core of the pigment particle (spectra 1 in Figures 6) or deeper in the orpiment containing layer (1 and 2 in Figure 7). All of these observations are consistent with the light-induced nature of the structural rearrangement observed in the natural orpiment leading to the As-As bonds. Similarly to what has been described for the realgar-pararealgar transformation, the formation of As-As bonds as well as the formation of $As_2O_3$ which may be simultaneous are not expected to change the arsenic oxidation state, which remains +3. A change in oxidation state would only be expected with the transformation of hydrated arsenic oxide (+3) in arsenates (+5).[18,19,34]

However, when exposed to blue laser light, no split is observed for the $AsS_{3/2}$ pyramids contribution, only a general decrease in the Raman signal for natural orpiment is observed (Figure 9d), which may indicate the formation of a poor Raman scattering phase. Similar to when exposed to the green laser, no arsenolite was identified during the experiment by its 367 $cm^{-1}$ band. The 368 $cm^{-1}$ band observed in Figure 9b is more likely characteristic of the orpiment as it is present before laser illumination and does not appear affected during the experiment. The formation of arsenolite is normally expected

upon light exposure of orpiment even though neither identified in the historical and mock-up paint samples, nor in the Raman - electrochemical coupled set-up experiments.[6,18,19,21] However, according to the Pourbaix diagram of dissolved As-species presented in Figure 10a, upon formation, due to its high solubility in aqueous solution, the arsenic oxide would dissolve and be present in $H_3AsO_3$ form, hardly identifiable in Raman analysis of an aqueous system. Furthermore, the formation of soluble arsenic oxide resulting from the breakdown of the natural orpiment would explain the decreasing Raman signal for the pigment observed in the time-dependent Raman experiment presented in Figure 9d.

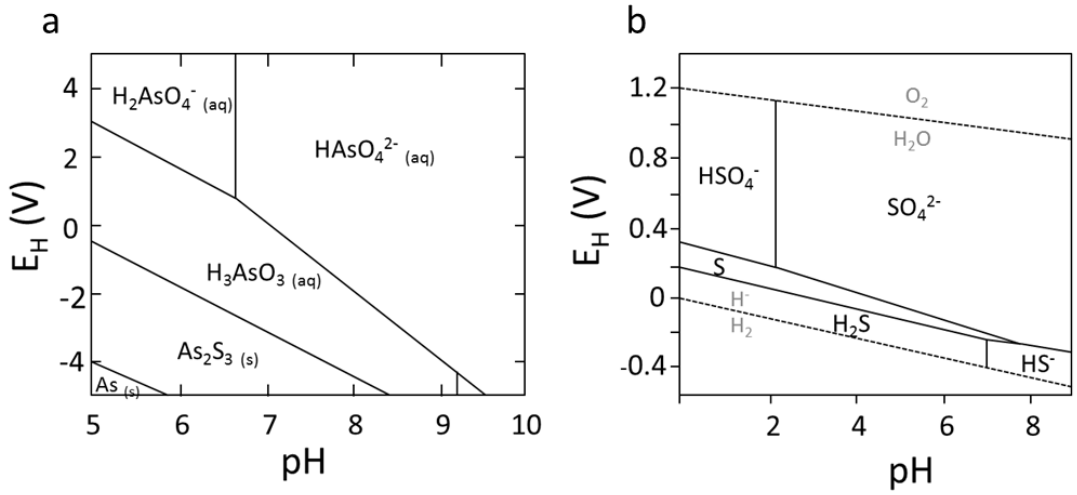


**Figure 10. Pourbaix diagrams of a) the arsenic system and b) the sulfur system, both showing the potential oxidation products than can be expected in the degradation of arsenic sulfide pigments.**

Since the As-As bond formation is only observed upon green laser exposure and not upon blue light illumination (Figure 9d), the influence of the wavelength (or energy per photon) as well as the laser power was investigated. For this purpose, three dry natural orpiment pigment grains were irradiated with 1) a 30 mW green (532 nm) laser and 2) a 30mW and a 12 mW blue (405 nm) laser. Raman spectra were measured before and after 50 hours of light exposure in order to assess the changes in the crystal structure (Figure 11). The pattern was decomposed as a sum of Gaussian peaks using the OriginPro8 software multiple peak fitting option. Two contributions were identified at 355 and 359 $cm^{-1}$. The full band integrations are given in Table 2. The later table also presents the ratios of the area of each contribution (355 and 359 $cm_{-1}$) to that of the total band area before and after illumination.

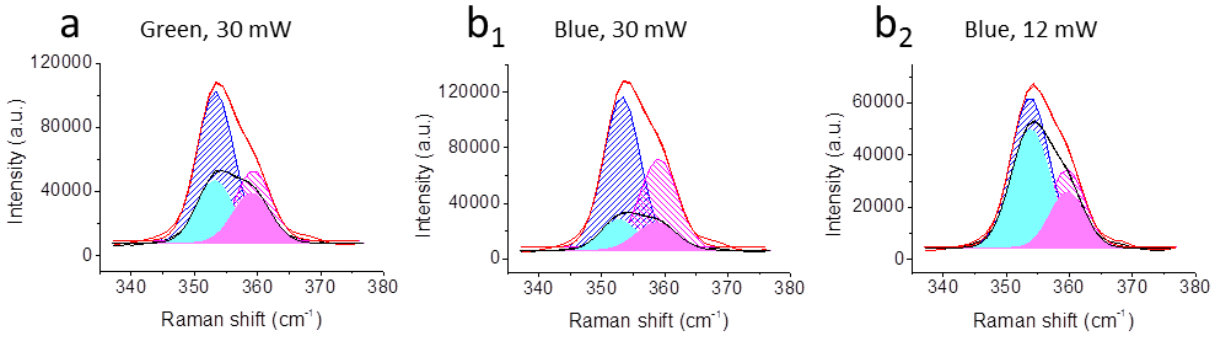


**Figure 11. Raman spectra of natural orpiment recorded before (red curve) and after (black curve) a) 30 mW blue (405 nm), b) 30 mW green (534 nm) and c) 12 mW blue (405 nm) laser illumination. The multiplet can be described as the sum of two Gaussian bands centered at 355 (cyan) and 359 $cm^{-1}$ (magenta). Cross-hatches Gaussians: contributions for the non-aged samples; filled Gaussians: contributions for aged paint samples.**

The Raman spectra and the total band integrations are showing a net intensity decrease for all bands for samples exposed to both 30 mW lasers (Figure 11a and Figure 11$b_1$). However, despite a general decrease of all band intensities, the relative contributions of the As-As bands at 359 $cm^{-1}$ appear to increase, thus creating a broadening of the of the characteristic $AsS3_{/2}$ pyramid band. No significant broadening of the $AsS_{3/2}$ pyramid band nor an increase of the As-As band is observed after illumination with the 12 mW blue laser (see ratios and FWHM values in Table 2). Hence, despite the slight decrease in Raman signal, no structural modification appears induced by the 12 mW blue laser. This strongly suggests that the formation of the As-As bond within the orpiment crystalline structure is not so strongly wavelength dependent but mostly power- or heat-induced.

**Table 2. Full band area, area ratios of the 359 $cm^{-1}$ and 355$cm^{-1}$ contribution to that of the total band area and FWHM values for both bands, before and after 50 hours of laser illumination of natural orpiment.**

| | | **a Green, 30 mW, 50 h** | | **b1 Blue, 30 mW, 50 h** | | **b2 Blue, 12 mW, 50 h** | |
|---|---|---|---|---|---|---|---|
| | | Before aging | After aging | Before aging | After aging | Before aging | After aging |
| Full band area | | 986580 | 511005 | 1251323 | 317927 | 637864 | 499572 |
| Area ratios | 355 $cm^{-1}$ | 0.69 | 0.55 | 0.62 | 0.50 | 0.67 | 0.70 |
| | 359 $cm^{-1}$ | 0.31 | 0.45 | 0.38 | 0.50 | 0.33 | 0.30 |
| FWHM | 355 $cm^{-1}$ | 6.93 | 6.77 | 6.86 | 6.97 | 7.19 | 7.37 |
| | 359 $cm^{-1}$ | 6.81 | 7.12 | 7.05 | 7.68 | 6.68 | 6.60 |

3. Fate of sulfur species in light-altered natural orpiment

Along with the identification of the As-As covalent bond via Raman spectroscopy, the fate of the sulfur that is released by the arsenic sulfide pigment was monitored using µ-XANES at the sulfur K-edge on historical samples H1 and H3. µ-XANES line scans were performed from the core (H1-a, H3-a)

to the shell (H1-e, H3-d) of the pigment particle. The XANES spectra for H1 and H3 are presented in Figure 12.

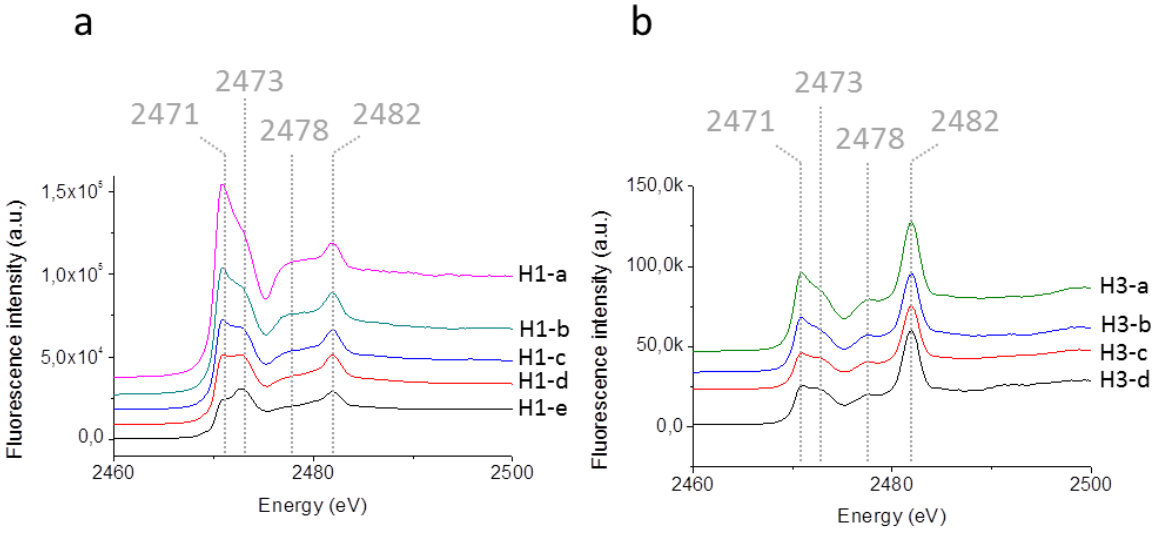


**Figure 12. XANES line scans from core (locations H1-a and H3-a) to shell (locations H1-e and H3-d) for the a) H1 and b) H3 paint samples (see also Figures 4ab). Both line scans show an increasing contribution at 2473 eV when moving from the core toward the superficial layers of the pigment grains. Other transitions correspond to S in the sulfidic (S2-, 2471 eV), sulfoxide (?) (S4+?, 2478 eV) and the sulfate (S6+, 2482 eV) states.**

Four main contributions are identified: 2471 eV ($En_1$), 2473 eV ($En_2$), 2478 eV ($En_3$) and 2482 eV ($En_4$) which respectively correspond to sulfide species (natural orpiment)[19], thiols or sulfur-containing organic compound(s) such as disulfides, DL-cystine or DL-methionine[35,36], possibly sulfoxide[19,36] and sulfate compounds[19], one of the expected degradation products of arsenic sulfide pigments.[35–37] While, according to the Pourbaix diagram presented in Figure 10b, the presence of sulfate species is to be expected, the presence of sulfur-containing organic compounds is unanticipated, especially as most of the sulfur-containing found in this energy range correspond to sulfur-containing amino-acids, not expected in gum arabic or oil medium. The XANES data also implies that the compound found at 2473 eV appears to be depth dependent: at the surface, a higher intensity is observed. In order to assess the evolution of the latter contribution (2473 eV) while moving from the core to the shell of the pigment particles, the ratios between the band intensity of the organosulfur compound(s) (2473 eV) and sulfide species (2471 eV) is listed in Table 3, for samples H1 and H3.

**Table 3. Evolution of the band intensity ratio of organosulfur to sulfide species from the core to the shell of the C1 and C3 pigment grains. (n/m: not measured).**

| | | H1 | H3 |
|---|---|---|---|
| Core | a | 0.79 | 0.82 |
| ↓ | b | 0.86 | 0.82 |
| ↓ | c | 0.92 | 0.90 |
| ↓ | d | 1.00 | 0.94 |
| Shell | e | 1.26 | n/m |

The results show that the sulfur-containing organic compounds abundance increases while that of the sulfides decreases when moving toward the outer shell of the pigment grains. At the light-exposed surface, more compounds characterized by the 2473 eV white line are formed. A similar observation was made for the As-As bond observed in the same samples, linking both phenomena.

Due to the light-induced nature of radical species and the increase in the 2473 eV signal in the most light-exposed area of the pigment grains, the hypothesis of sulfur radicals' formation during the light-induced aging of natural orpiment cannot be ruled out. However, due to the great reactivity of these compounds[38], they are very unlikely to be found in the analyzed samples but are most likely involved in the formation of di- or polysulfide compounds as suggested by the XANES data. Due to the weak S-S bond, a decomposition of organosulfur compounds will often follow[39]. This decomposition may be at the origin of the rotten egg odor witnessed during the sampling as polysulfide are considered to be potentials precursors of hydrogen sulfide ($H_2S$)[40].

Therefore, a similar process as the one described for the second step of the transformation of realgar to pararealgar (Figure 1) can be foreseen for natural orpiment in which, under the influence of light, sulfur atoms would be released in favor of the formation of As-As bonds. The homopolar bond being weaker than the shorter As-O bond[41], the arsenic-rich compound formed is expected to be oxidized into $As_2O_3$, as observed during the oxidation process of pure arsenic. Meanwhile, the sulfur atoms released, possibly very reactive radicals, could then react with their organic-rich surrounding environment to form organosulfur compounds, which may lead to the formation of volatile hydrogen sulfide[40]. The formation of hydrogen sulfide is consistent with the rotten egg odor witnessed when opening the storage boxes of the mock-ups paint samples and also explains the non-contact darkening of the Cu- or Pb-containing pigment when present nearby (Figure 3) by inducing the formation of dark copper and lead sulfide species. Furthermore, the lack of identification of any other inorganic phase but natural orpiment and arsenic oxide in the μ-XRPD analyses performed also supports this possibility.

**Conclusion**

While degradation of natural orpiment, a yellow arsenic sulfide, is described as rather straightforward and exclusively leading to arsenic oxide and arsenate species, combination of Raman spectroscopy, time dependent Raman spectroscopy-electrochemistry and x-ray absorption near edge structure investigations on natural orpiment-containing historical samples, natural orpiment mock-up samples and unbound natural orpiment demonstrated the existence, next to the formation of $As_2O_3$, of a light-induced intermediate secondary phase that is characterized by As-As bonds in Raman spectroscopy. Due to a greater stability of the As-O bond compared to As-As, the metastable arsenic-rich compounds will later on transform into arsenic oxide, the known degradation product of natural orpiment. During this degradation process, similarly to what has been previously observed for natural realgar, a structural rearrangement takes place in which sulfur atoms (possibly radicals) are released. Depending on the environmental conditions, these sulfur atoms released can react with their surroundings and form organosulfur materials, which may lead to the formation of hydrogen sulfide. The production of the latter compounds following the structural rearrangement observed in natural orpiment can explain the well-documented darkening of copper- and lead-containing paint

samples under the influence of adjacent arsenic sulfides paints via the formation of copper or lead sulfides.

**Acknowledgements**

This research is made possible with the support of the Belgian Science Policy Office (BELSPO, Brussels) through the research program Science for a Sustainable Development – SDD, "Long-term role and fate of metal-sulfides in painted works of art – S2ART" (SD/RI/04A). We gratefully acknowledge Julie Arslanoglu (Conservation and Scientific Research Department at the Metropolitan Museum of Art, New York, NY, USA) for having providing us the orpiment, verdigris and minium mock-up samples. The authors greatly acknowledge the Paul Scherrer Institut, Villigen, Switzerland and the German Electron Synchrotron (DESY) for provision of synchrotron radiation beamtimes at respectively beamline Phoenix of the SLS and Petra III.

**References**

[1] L. Zanella, F. Casadio, K. A. Gray, R. Warta, Q. Ma, J.-F. Gaillard, *J. Anal. At. Spectrom.* **2011**, *26*, 1090–1097.
[2] J. Mass, J. Sedlmair, C. S. Patterson, D. Carson, B. Buckley, C. Hirschmugl, *The Analyst* **2013**, *138*, 6032.
[3] G. Van der Snickt, J. Dik, M. Cotte, K. Janssens, J. Jaroszewicz, W. De Nolf, J. Groenewegen, L. Van der Loeff, *Anal. Chem.* **2009**, *81*, 2600–2610.
[4] G. Van der Snickt, K. Janssens, J. Dik, W. De Nolf, F. Vanmeert, J. Jaroszewicz, M. Cotte, G. Falkenberg, L. Van der Loeff, *Anal. Chem.* **2012**, *84*, 10221–10228.
[5] A. Wallert, **1984**.
[6] E. W. FitzHugh, in *Artists Pigments Handb. Their Hist. Charact. Vol 3* (Ed.: E.W. FitzHugh), National Gallery Of Art, Washington, **1997**, pp. 47–79.
[7] N. Strbac, I. Mihajlovic, D. Minic, D. Zivkovic, Z. Zivkovic, *J. Min. Metall. Sect. B Metall.* **2009**, *45*, 59–67.
[8] V. S. F. Muralha, C. Miguel, M. J. Melo, *J. Raman Spectrosc.* **2012**, *43*, 1737–1746.
[9] D. Saunders, J. Kirby, *Natl. Gallery Tech. Bull.* **2004**, *25*, 62–72.
[10] M. Douma, in *Pigments Ages*, **2008**.
[11] C. Miguel, A. Claro, A. P. GonÃ§alves, V. S. F. Muralha, M. J. Melo, *J. Raman Spectrosc.* **2009**, *40*, 1966–1973.
[12] R. J. Gettens, G. L. Stout, *Painting Materials: A Short Encyclopaedia*, Dover, New York, NY, **1966**.
[13] V. Daniels, B. Leach, *Stud. Conserv.* **2004**, *49*, 73–84.
[14] L. Bindi, P. Bonazzi, *Am. Mineral.* **2007**, *92*, 617–620.
[15] K. Trentelman, L. Stodulski, M. Pavlosky, *Anal. Chem.* **1996**, *68*, 1755–1761.
[16] D. L. Douglass, C. Shing, G. Wang, *Am. Mineral.* **1992**, *77*, 1266–1274.
[17] M.-C. Corbeil, K. Helwig, *Stud. Conserv.* **1995**, *40*, 133.
[18] M. Vermeulen, G. Nuyts, J. Sanyova, A. Vila, D. Buti, J.-P. Suuronen, K. Janssens, *J. Anal. At. Spectrom.* **2016**, *31*, 1913–1921.
[19] K. Keune, J. Mass, F. Meirer, C. Pottasch, A. van Loon, A. Hull, J. Church, E. Pouyet, M. Cotte, A. Mehta, *J. Anal. At. Spectrom.* **2015**, *30*, 813–827.
[20] A. Kyono, M. Kimata, T. Hatta, *Am. Mineral.* **2005**, *90*, 1563–1570.
[21] A. Macchia, L. Campanella, D. Gazzoli, E. Gravagna, A. Maras, S. Nunziante, M. Rocchia, G. Roscioli, *Procedia Chem.* **2013**, *8*, 185–193.
[22] M. Pagliai, P. Bonazzi, L. Bindi, M. Muniz-Miranda, G. Cardini, *J. Phys. Chem. A* **2011**, *115*, 4558–4562.

[23] L. Bindi, V. Popova, P. Bonazzi, *Can. Mineral.* **2003**, *41*, 1463–1468.
[24] M. Vermeulen, J. Sanyova, K. Janssens, *Herit. Sci.* **2015**, *3*, DOI 10.1186/s40494-015-0040-7.
[25] A. R. Kampf, R. T. Downs, R. M. Housley, R. A. Jenkins, J. Hyrsl, *Mineral. Mag.* **2011**, *75*, 2857–2867.
[26] W. Anaf, S. Trashin, O. Schalm, D. van Dorp, K. Janssens, K. De Wael, *Anal. Chem.* **2014**, *86*, 9742–9748.
[27] W. Anaf, O. Schalm, K. Janssens, K. De Wael, *Dyes Pigments* **2015**, *113*, 409–415.
[28] E. Ayalew, K. Janssens, K. De Wael, *Anal. Chem.* **2016**, *88*, 1564–1569.
[29] B. Ravel, M. Newville, *J. Synchrotron Radiat.* **2005**, *12*, 537–541.
[30] J.-L. Adam, X. Zhang, *Chalcogenide Glasses: Preparation, Properties and Applications*, Woodhead Publishing, **2014**.
[31] M. Dussauze, X. Zheng, V. Rodriguez, E. Fargin, T. Cardinal, F. Smektala, *Opt. Mater. Express* **2012**, *2*, 45–54.
[32] R. Schäfer, P. Schmidt, Eds. , *Methods in Physical Chemistry*, Wiley-VCH, Weinheim, Germany, **2012**.
[33] P. J. Aarnoutse, J. A. Westerhuis, *Anal. Chem.* **2005**, *77*, 1228–1236.
[34] K. Keune, J. Mass, A. Mehta, J. Church, F. Meirer, *Herit. Sci.* **2016**, *4*, DOI 10.1186/s40494-016-0078-1.
[35] G. Sarret, J. Connan, M. Kasrai, G. M. Bancroft, A. Charrié-Duhaut, S. Lemoine, P. Adam, P. Albrecht, L. Eybert-Bérard, *Geochim. Cosmochim. Acta* **1999**, *63*, 3767–3779.
[36] A. Vairavamurthy, *Spectrochim. Acta. A. Mol. Biomol. Spectrosc.* **1998**, *54*, 2009–2017.
[37] A. A. Gambardella, C. M. Schmidt Patterson, S. M. Webb, M. S. Walton, *Microchem. J.* **2016**, *125*, 299–307.
[38] M. Lazár, Ed. , *Free Radicals in Chemistry and Biology*, CRC Press, Boca Raton, Fla, **1989**.
[39] A. G. Vandeputte, M. K. Sabbe, M.-F. Reyniers, G. B. Marin, *Chem. - Eur. J.* **2011**, *17*, 7656–7673.
[40] R. Tocmo, D. Liang, Y. Lin, D. Huang, *Front. Nutr.* **2015**, *2*, DOI 10.3389/fnut.2015.00001.
[41] J. A. Dean, N. A. Lange, Eds. , *Lange's Handbook of Chemistry*, McGraw-Hill, New York, NY, **1999**.